Stem Cell Research & Therapy

RESEARCH

Open Access

Single-cell dissection reveals promotive role of *ENO1* in leukemia stem cell self-renewal and chemoresistance in acute myeloid leukemia

Yun Tian[1,2,3†], Jiafan Guo[2,4†], Lipeng Mao[3†], Zhixi Chen[1,2†], Xingwei Zhang[2,4], Yangqiu Li[1,2*], Yikai Zhang[1,2,5*], Xianfeng Zha[4*] and Oscar Junhong Luo[3*]

Abstract

Background Quiescent self-renewal of leukemia stem cells (LSCs) and resistance to conventional chemotherapy are the main factors leading to relapse of acute myeloid leukemia (AML). Alpha-enolase (*ENO1*), a key glycolytic enzyme, has been shown to regulate embryonic stem cell differentiation and promote self-renewal and malignant phenotypes in various cancer stem cells. Here, we sought to test whether and how *ENO1* influences LSCs renewal and chemoresistance within the context of AML.

Methods We analyzed single-cell RNA sequencing data from bone marrow samples of 8 relapsed/refractory AML patients and 4 healthy controls using bioinformatics and machine learning algorithms. In addition, we compared *ENO1* expression levels in the AML cohort with those in 37 control subjects and conducted survival analyses to correlate *ENO1* expression with clinical outcomes. Furthermore, we performed functional studies involving *ENO1* knockdown and inhibition in AML cell line.

Results We used machine learning to model and infer malignant cells in AML, finding more primitive malignant cells in the non-response (NR) group. The differentiation capacity of LSCs and progenitor malignant cells exhibited an inverse correlation with glycolysis levels. Trajectory analysis indicated delayed myeloid cell differentiation in NR group, with high *ENO1*-expressing LSCs at the initial stages of differentiation being preserved post-treatment. Simultaneously, *ENO1* and stemness-related genes were upregulated and co-expressed in malignant cells during early differentiation. *ENO1* level in our AML cohort was significantly higher than the controls, with higher levels in NR compared to those in complete remission. Knockdown of *ENO1* in AML cell line resulted in the activation of LSCs, promoting cell differentiation and apoptosis, and inhibited proliferation. *ENO1* inhibitor can impede the proliferation of AML cells. Furthermore, survival analyses associated higher *ENO1* expression with poorer outcome in AML patients.

[†]Yun Tian, Jiafan Guo, Lipeng Mao and Zhixi Chen authors contributed equally to this work.

*Correspondence:
Yangqiu Li
yanqiuli@hotmail.com
Yikai Zhang
jnuyikaizhang@163.com
Xianfeng Zha
zhaxianfeng_0@163.com
Oscar Junhong Luo
luojh@jnu.edu.cn
Full list of author information is available at the end of the article

Conclusions Our findings underscore the critical role of *ENO1* as a plausible driver of LSC self-renewal, a potential target for AML target therapy and a biomarker for AML prognosis.

Keywords *ENO1*, AML, LSCs, Chemoresistance, Single-cell RNA sequencing

Introduction

Acute Myeloid Leukemia (AML) is the most common acute leukemia in adults, characterized by abnormal proliferation of leukemic blasts and differentiation arrest [1, 2]. Despite the development of various targeted therapies, the treatment of most AML patients, excluding those with acute promyelocytic leukemia, largely relies on the standard '7 + 3' chemotherapy regimen and hematopoietic stem cell transplantation (HSCT) [3, 4]. However, treatment outcomes for AML remain unsatisfactory, with a significant number of patients experiencing chemotherapy resistance and relapse after remission [2, 5]. The primary cause of AML refractoriness and relapse is the leukemia stem cells (LSCs), which possess long-term self-renewal capability [6, 7]. Conventional therapies can destroy the bulk of leukemic blasts but fail to eradicate LSCs, which can alter their state during dormancy and reinitiate malignancy [8, 9]. To date, cell surface proteins are most commonly used to identify stem cells, often through flow cytometry or related methods. The primary marker used for identifying and enriching LSCs is $CD34^{+}CD38^{-}$, the same as for hematopoietic stem cells (HSCs) [10]. Several other markers, including CD99, TIM3, GPR65, CD82, and CD9, are upregulated in LSCs compared to normal HSCs [11–14]. However, in the complex context of cancer, surface marker expression can vary between patients and even within the same patient during pathogenesis [15, 16]. Hence, LSCs are difficult to isolate due to their scarcity, significant similarity to healthy HSCs, and phenotypic plasticity, resulting in the lack of universal surface markers for LSCs [8, 17]. Therefore, one of the critical issues in AML treatment is identifying and targeting key molecules that specifically regulate the self-renewal of AML LSCs.

Glycolysis represents a central metabolic pathway in all organisms, crucial for stem cell differentiation and cancer biology [18, 19]. Cancer cells, in particular, preferentially choose the relatively inefficient aerobic glycolysis pathway (Warburg effect) over the energy-efficient oxidative phosphorylation (OXPHOS) pathway [20]. Embryonic pluripotent stem cells must utilize glycolysis to meet the demands of continuous self-renewal, providing building blocks for the biosynthesis of nucleotides, peptides, and lipids [21]. Although stemness requires glycolysis, lineage differentiation involves a shift towards OXPHOS [22]. Alpha-Enolase, or enolase 1 (*ENO1*), is a key enzyme in the glycolytic pathway, catalyzing the reversible interconversion between 2-phosphoglycerate (2-PG) and phosphoenolpyruvate (PEP) [21, 23]. In malignant cells, *ENO1* is typically overexpressed and is a multifunctional protein with oncogenic properties, including accelerating glycolysis, promoting cancer cell proliferation, migration, invasion, drug resistance, and activating oncogenic signaling pathways [24–26]. Recent studies have identified high *ENO1* expression in AML and myelodysplastic syndromes through bulk detection methods, recognizing it as a predictor of poor prognosis [27–30]. Despite extensive research on the role of *ENO1* in solid tumors and its emerging relevance in leukemia, the mechanisms through which *ENO1* leads to unfavorable outcomes in AML remain unclear.

Single-cell RNA sequencing (scRNA-seq) technology is a powerful approach for cancer research, playing a crucial role in uncovering tumor heterogeneity, deepening the understanding of tumor biology, and guiding personalized therapies. scRNA-seq combined with chromosomal copy number variations (CNVs) analysis methods (e.g., CopyKAT and IfCNV) [31, 32], and/or tumor marker gene expression have been used extensively for identifying tumor cells [33]. However, compared to solid tumors, CNVs is less frequent in AML, and constructing classifiers based on marker genes to identify leukemia cells may lead to significant errors, as AML cell diversity partly reflects a re-interpretation of myeloid development [34–36]. This complexity makes it difficult to accurately distinguish LSCs from normal HSCs. Therefore, accurately inferring AML tumor cells using scRNA-seq data remains a significant challenge. To this end, we innovatively combined scRNA-seq data with machine learning techniques to model and infer malignant cell populations in AML.

To test whether and how *ENO1* influences AML patients, it is imperative to delve into specific cell types affected by *ENO1* and explore its precise mechanisms in the pathophysiology of AML during disease progression. Such investigations will provide deeper insights and theoretical foundations for developing more effective treatment strategies. Our findings revealed that *ENO1* plays a critical role in maintaining the self-renewal and survival of AML stem cells. Additionally, our data suggest that *ENO1* levels could serve as a peripheral biomarker for monitoring AML status in clinical settings, providing a straightforward method to track disease progression and response to treatment. Collectively, these observations

strongly support the development of *ENO1* inhibitors as a novel therapeutic strategy to target the self-renewal of LSCs in AML patients.

Methods

Clinical sample collection

Peripheral blood from 28 newly diagnosed patients with AML and 37 healthy individuals were collected for quantitative reverse transcription polymerase chain reaction (qRT-PCR) [37]. Samples were obtained in The Hematology Department, First Affiliated Hospital of Jinan University. Ethical approval was obtained from the Ethics Committee of the School of Medicine of Jinan University, and informed consent was provided by the patients and healthy donors.

Cell culture and treatment

AML cell line MOLM-13 was cultured in RPMI 1640 (Gibco) containing 10% fetal bovine serum (Zeta life) at 37 °C in a 5% CO_2 atmosphere. Cells were passaged at a 1:3 ratio to ensure they were in the logarithmic growth phase. MOLM-13 cells were treated with different concentrations of AP3-III-a4 (0 μM, 0.625 μM, 1.25 μM, 2.5 μM, 5 μM and 10 μM) for different periods of time (0 h, 24 h, 48 h, 72 h and 96 h), and cell proliferation was detected by cell counting kit-8 (CCK8).

Construction of *ENO1* knockdown cell line

The *ENO1* short hairpin RNA (shRNA) expression vectors were constructed and packaged as lentivirus (Miaoling Biology, Wuhan, China). MOLM-13 cells in logarithmic growth phase were used and infected with the lentivirus for 12 h, and then replaced with new complete medium for a further 48 h. After 48 h, positive clones were screened with puromycin (2 μg/mL). The *ENO1* knockdown efficiency was verified by western blotting (WB) and qRT-PCR [37, 38]. The cell proliferation differences were determined by CCK8.

RNA extraction, qRT-PCR, and bulk RNA-seq

Total RNA extraction and cDNA synthesis were performed as previously described [39]. The oligonucleotide sequences of *ENO1* were ENO1-F 5'-GCCGTGAACGAGAAGTCCTG-3' and ENO1-R 5'-AGGTATCTTCAGTCTCCCCCG-3'. *ACTB* (β-actin) was employed as the control gene, with the oligonucleotide sequences ACTB-F 5'-TTGTTACAGGAAGTCCCTTGCC-3' and ACTB-R 5'-ATGCTATCACCTCCCCTGTGTG-3'. RNA quality and concentration were assessed using NanoDrop 2000 and Agilent 2100 Bioanalyzer [40]. We conducted bulk RNA-seq on MOLM-13 cells before and after stable knockdown of *ENO1*, with repeated experiments and triplicate samples to minimize errors. The extraction and detection of RNA-seq in the samples were performed by Wuhan Metware Biotechnology Co., Ltd. (Wuhan, China; www.metware.cn). Data analysis was conducted using the STAR aligner and DESeq2 for differential expression analysis.

CCK8 assay for cell proliferation

The cells were seeded in 96-well plates at a density of 4000 cells per well with the addition of various concentrations of AP3-III-a4 (0 μM, 0.625 μM, 1.25 μM, 2.5 μM, 5 μM and 10 μM), and incubated for 0, 24, 48, 72, and 96 h. At each time point, 10 μL of CCK-8 reagent was added. Cells were incubated for 2 h at 37 °C. Absorbance was measured at 450 nm using a microplate reader. Each group had three replicates, and experiments were repeated three times.

Western blotting

The *ENO1* stable knockdown cells were collected, total protein was extracted from cells and quantified using a BCA protein assay kit (Hangzhou Fude Biological technology Co., Ltd.). Thirty micrograms of protein were separated by SDS-PAGE and transferred to PVDF membranes [41]. Membranes were blocked with 5% non-fat milk for 1 h. Primary antibodies against ENO1 (1:1000, Proteintech) and β-actin (1:5000, Proteintech) were incubated overnight. The next day, HRP-conjugated secondary antibodies (1:10000, Proteintech) were incubated for 1 h. ECL chemiluminescent reagent was used for detection, and images were captured using a gel imaging system.

scRNA-seq data download and processing

We downloaded two sets of scRNA-seq data from the GEO database: GSE223844 (comprising data from 8 relapsed/refractory (R/R) AML patients) and GSE116256 (comprising healthy controls (HCs) and predictive data) [1, 42]. Eight AML patients were either in relapsed or refractory states. All scRNA-seq data were obtained from adult (≥18 years old) bone marrow (BM) samples. All patients were being treated with the same regimen, consisting of decitabine (20 mg/m^2 on days 1–5) and ipilimumab (3–10 mg/m^2 on day 1) [42]. Among them, three patients have achieved complete remission (CR) after treatment, while five patients are classified as non-response (NR). The clinical characteristics of the patients and information on HCs are provided in Supplementary Table S1. The downloaded data were first imported into the R environment and processed using the Seurat package (version 4.1.0) [43]. Initial processing steps included creating Seurat objects from the expression matrices, quality control to filter out low-quality cells and genes (with criteria of 200–4000 genes per cell and less than

5% mitochondrial gene content per cell), data normalization using the LogNormalize method, and selecting and scaling the top 2000 variable genes. To integrate data from different sources, we employed the Harmony method within Seurat for batch effect correction and data integration (Harmony version 0.1.0). Specifically, the GSE223844 and GSE116256 datasets were merged to create a unified Seurat object, followed by batch effect correction using Harmony (version 0.1.0), which iteratively reconciles differences across batches in the latent space [44]. Subsequently, dimensionality reduction was performed using Principal Component Analysis (PCA), selecting the top 20 principal components for further analysis. Clustering analysis was conducted, and non-linear dimensionality reduction techniques such as UMAP were applied to visualize the distribution of different cell populations. Cell types were annotated using known marker genes.

Pseudotime analysis

To investigate the cell differentiation trajectory, we performed pseudotime analysis using both Monocle (version 2.22.0) and Monocle3 (version 1.3.5). For Monocle, the specific steps involved converting Seurat objects into Monocle objects while retaining highly variable genes and cell annotation information [45]. Trajectory inference was conducted using Monocle's DDRTree method for dimensionality reduction and trajectory inference, resulting in the visualization of cell differentiation trajectories. We analyzed the differentiation dynamics along the pseudotime trajectory for both normal and malignant cells, comparing gene expression levels under different patient conditions. Additionally, heatmaps were generated to visualize the expression patterns of key genes across the pseudotime trajectory, providing a comprehensive view of gene expression dynamics during cell differentiation. In addition, we also utilized Monocle3 for pseudotime analysis [46]. The steps for Monocle3 are similar, involving the conversion of Seurat objects into Monocle3's specialized objects, retention of highly variable genes and cell annotation information, and trajectory inference using Monocle3's methods. Monocle3 provides advanced features for trajectory analysis, such as improved dimensionality reduction algorithms and enhanced visualization capabilities.

Machine learning analysis

To develop a classifier capable of accurately identifying malignant cells based on transcriptional features, we utilized supervised machine learning methods, specifically employing the XGBoost algorithm [47]. The classifier was trained on scRNA-seq data with malignant markers (GSE116256) and its performance was validated using receiver operating characteristic (ROC) analysis, with the area under the curve (AUC) being calculated to quantify the classifier's accuracy. Following validation, the classifier was applied to the GSE223844 dataset to identify malignant cells among HCs, CR patients, and NR patients.

Regulatory proteins analysis

To identify and analyze key regulatory proteins involved in the regulation of gene expression in malignant cells, we employed the VIPER (Virtual Inference of Protein-Activity by Enriched Regulon analysis) algorithm [48]. VIPER is a powerful computational approach that infers the activity of regulatory proteins, from gene expression data by analyzing 'regulons'—groups of target genes regulated by the same regulatory proteins. By assessing the coordinated expression changes in these target genes, VIPER infers the activity levels of the regulatory proteins, providing insights into the regulatory mechanisms driving malignancy. This approach was used to compare and validate the inferred regulatory protein activities between normal and malignant cells. Additionally, heatmaps were generated to cluster the related regulatory proteins in CR and NR groups, visualizing the differential regulatory profiles associated with distinct patient outcomes.

Network construction

To construct a gene regulatory network (GRN) for differentially expressed genes (DEGs) and identify central regulator protein (such as *ENO1*, *SREBF1*, and *TCF4*), we utilized VIPER and Cytoscape [49]. The regulatory model is based on the ARACNe-inferred interactome, provided in the build-in function of the VIPER R package. These inferred interactions and activities were then visualized and analyzed using Cytoscape, a platform for network analysis and visualization.

Gene ontology enrichment analysis and pathway scoring

To analyze the biological processes enriched in DEGs, we used the clusterProfiler package [50]. This tool allows for systematic analysis of gene ontology (GO) terms to determine significantly overrepresented biological processes, molecular functions, and cellular components in DEGs. Additionally, we employed Gene Set Variation Analysis (GSVA) for GO enrichment analysis to assess the biological processes enriched in DEGs [51]. This approach enables us to comprehensively understand the functional impact of DEGs through the enrichment of gene sets. Furthermore, we used Seurat AddModuleScore function to score cells based on specific gene sets. This method allows us to quantify the activity of particular pathways or gene sets within individual cells, providing deeper insights into the functional implications of DEGs.

Bulk RNA-seq analysis

For the upstream analysis of bulk RNA-seq data, we first used Cutadapt to trim low-quality bases and adapter sequences from the raw sequencing reads. The trimmed reads were then aligned to the reference genome (hg38) using aligner HISAT2. Transcript assembly and quantification were performed using featureCounts to generate raw count data. Finally, the raw count data were normalized, and differential expression analysis was conducted using DESeq2 to identify DEGs between the knockdown and control groups [52]. Heatmaps were generated using pheatmap, and clustering of the data was performed using mfuzz [53].

Bulk RNA-seq stemness scoring

To assess the changes in stemness following *ENO1* knockdown in leukemia, we performed RNA-seq on *ENO1* knockdown leukemia cell lines. For LSC scoring, we downloaded gene sets from Dick et al. article, specifically dataset GSE153917, which includes differentially expressed genes between Long-Term Hematopoietic Stem Cell (LT-HSC) activated and quiescent states [54]. Using GSVA, we scored the enrichment of these LSC gene sets in the RNA-seq data. GSVA is a non-parametric, unsupervised method that estimates the variation in pathway activity over a sample population, providing insights into the functional impact of *ENO1* knockdown on LSC-related pathways.

Survival curve analysis

We used the GEPIA tool to obtain gene expression and survival data for AML patients from the TCGA database [55]. In the 'Survival Analysis' module of GEPIA, target gene lists (e.g., *ENO1*, etc.) were used as input, group parameters (50% cutoff) were set, AML patient cohorts were selected, and survival types (e.g., Overall Survival) were chosen. GEPIA generated Kaplan–Meier survival curves and used Log-rank tests to evaluate the relationship between the expression levels of these genes and patient prognosis. Additionally, we constructed an internal database cohort, including AML patient data from our clinical center. Using the same analytical methods, we evaluated the relationship between target gene expression levels and patient prognosis in our internal cohort.

Statistical methods

All statistical analyses were performed using R (version 4.1.0) and GraphPad Prism 9.0 software, including t-test, Fisher's exact test, Wilcoxon rank-sum test, Chi-square test, Kruskal–Wallis test, Kaplan–Meier survival curves, and the Log-rank test. All significance levels were indicated by *P*-values, with *P*-values < 0.05 considered statistically significant (*****P*-value < 0.0001, ****P*-value < 0.001, ***P*-value < 0.01, **P*-value < 0.05, ns: not significant).

Results

Cellular heterogeneity among R/R AMLs

To elucidate the cellular composition and functional characteristics of AML and to understand the mechanisms leading to poor prognosis, we analyzed scRNA-seq data of BM samples from 8 R/R AML patients and 4 HCs (Supplementary Table S1). Among all R/R AML patients treated with the same protocol (decitabine combined with ipilimumab), three achieved CR (CR group) while five were classified as NR group (see Methods Section for details). The analyzed scRNA-seq datasets consisted of 27,754 and 24,325 cells from pre-treatment R/R AML patients and HCs, respectively (Fig. 1A; Supplementary Fig. 1A).

We identified a variety of cell types based on characteristic cell markers, including hematopoietic stem cells/multipotent progenitors (HSC/MPPs), granulocyte-monocyte progenitors (GMPs), megakaryocyte-erythroid progenitors (MEPs), eosinophil, basophil, and mast cell

(See figure on next page.)

Fig. 1 Single-cell transcriptomic profiling elucidates the cellular heterogeneity of R/R AML patients. **A** UMAP visualization of scRNA-seq data of BM samples from AML patients and HCs. Each dot represents a single cell, colored by cell cluster. The clusters include hematopoietic stem cells/multipotent progenitors (HSC/MPPs), granulocyte-monocyte progenitors (GMPs), megakaryocyte-erythroid progenitors (MEPs), eosinophil, basophil, and mast cell progenitors (EBMs), erythrocytes (early, mid, and late Erys), monocytes, B cells, T cells, natural killer (NK) cells, conventional dendritic cells (cDCs), and plasmacytoid dendritic cells (pDCs). **B** Dot plot of average gene expression for cell type-specific genes. The average expression of selected marker genes is shown across different cell types. The color intensity represents the average expression level, and the size of the dot indicates the percentage of cells expressing the gene. All samples are used in cluster annotation based on cell types corresponding to A. **C** Proportion of distinct cell types in AML and healthy controls (HCs) samples. Bar plots display the proportion of each cell type in AML (purple) and HCs (blue) samples, highlighting the differences in cell type distribution. **D** Stacked bar plots displaying the composition of cell types in AML and HCs samples, with each color representing a different cell type, depicting the distribution within each sample type. **E.** UMAP visualization of cells from AML patients. The cells were categorized by patients with complete remission (CR) and non-response (NR) after chemotherapy. Cells from CR patients are highlighted in pink (top panel), while cells from NR patients are highlighted in purple (bottom panel), depicting the distribution and clustering of cells based on treatment response. **F**. Cell absolute counts (top panel) and relative abundances (bottom panel) of all cell types in AML patients. Different colors represent CR (pink) and NR (purple) samples. The bars in the bottom panel represent log2 odds ratios (Fisher exact test, *P*-value after Bonferroni correction; n.s., not significant; ****P* < .0001)

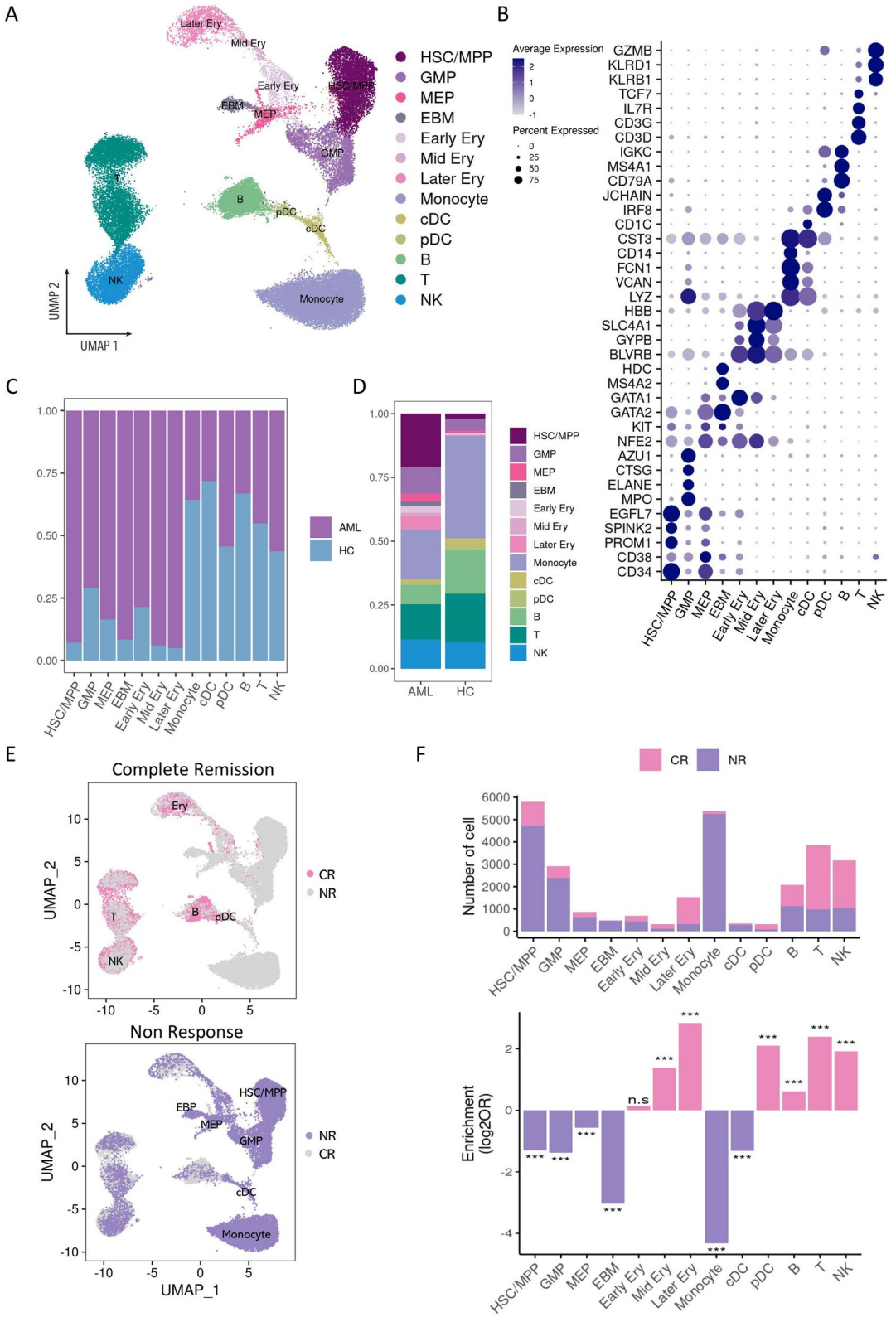

Fig. 1 (See legend on previous page.)

progenitors (EBMs), erythrocytes (early, mid, and late Erys), monocytes, B cells, T cells, natural killer (NK) cells, conventional dendritic cells (cDCs), and plasmacytoid dendritic cells (pDCs) (Fig. 1A, B). The HSC/MPPs cells exhibited high expression of *CD34*, *PROM1*, *SPINK2*, and *EGFL7*. Precursor cells GMPs and MEPs expressed *CD34* to varying degrees but were distinguished by their lineage-specific marker genes: *MPO*, *ELANE*, *CTSG*, *AZU1* for GMPs, and *NFE2*, *KIT*, *GATA2*, *GATA1* for MEPs. EBMs specifically exhibited high expression of *HDC* and *MS4A2*. Erythrocytes were classified into early, mid, and late stages, based on differential expression levels of *BLVRB*, *GYPB*, *SLC4A1*, and *HBB*. Myeloid cell populations were identified based on their specific markers, including monocytes (*LYZ*, *VCAN*, *FCN1*, and *CD14*), cDCs (*CST3* and *CD1C*), and pDCs (*IRF8* and *JCHAIN*). Additionally, three major lineages populations were recognized based on gene expression patterns: T cells (*CD3D*, *CD3G*, *IL7R*, and *TCF7*), B cells (*CD79A*, *MS4A1*, and *IGKC*), and NK cells (*KLRB1*, *KLRD1*, and *GZMB*). Additionally, the expression levels of lineage-specific marker genes, such as *CD38*, *AZU1*, *HDC*, *HBB*, *CST3*, *CD3G*, *KLRD1*, and *CD79A*, were consistent with the UMAP clustering data, validating our cell type annotations (Fig. 1B; Supplementary Fig. 1B).

There were significant differences in cell composition between R/R AML patients and HCs. Specifically, in AML patients, primitive and myeloid cells constitute on average 67.2%, with HSC/MPPs and GMPs comprising 20.9% and 10.4%, respectively. In contrast, HCs are primarily composed of monocytes (40.0%), with HSC/MPPs and GMPs accounting for 1.8% and 4.8%, respectively (Fig. 1C,D; Supplementary Fig. 2A). The cellular composition varies significantly among R/R AML patients, which may impact treatment outcomes. All cell types were present in both CR and NR patients, but there were significant differences in their abundance between the two groups (Fig. 1E, F; Supplementary Fig. 2B). Progenitor cells (such as HSC/MPPs, GMPs, MEPs, EBMs, Early Erys) and more mature myeloid cells (monocytes and cDCs) were enriched in NR patients, whereas samples from CR patients were enriched in late-stage erythroid cells, lymphoid cells (B, T, NK), and pDCs. The observation that R/R AML patients possess a higher proportion of primitive or progenitor cells, particularly those in the NR group, strongly suggests a potential association between cell composition and treatment response.

Negative correlation between glycolysis and cell differentiation in HSC/MPPs and GMPs of R/R AML

According to the scRNA-seq characterization, the majority of AML BM samples consisted of primitive and myeloid progenitor cells, particularly in patients from the NR group. Accurately distinguishing between normal and malignant cells is of great importance for a deeper understanding of the pathogenesis of AML and guiding treatment strategies [36]. However, because leukemia cells in AML resemble normal myeloid development and exhibit fewer CNVs mutations, methods used to infer tumor cells in solid tumors are not well-suited for hematologic malignancies [34–36].We employed a supervised machine learning approach to develop a classifier that inferred malignant cells from scRNA-seq data by learning from previously validated AML cell profiles [1]. The performance of the classifier was validated using ROC analysis, yielding an AUC of 0.99, indicating high accuracy and robustness (Fig. 2A; Supplementary Fig. 3A).

(See figure on next page.)

Fig. 2 Identification of malignant cells and comparison with normal hematopoietic cell lineages. **A** UMAP plots illustrating the distribution of malignant cells (red) and normal cells (gray) across different sample types (HC, CR, and NR). **B** Statistical comparison between malignant cells and normal cells. The top panel shows the absolute cell counts for cell types predicted to have more than 20% malignant cells, compared to the normal group. The bottom panel shows the relative abundances. Different colors represent the malignant cell (pink) and control (purple) groups. The bar plots in the bottom panel depict the log2 odds ratios (Fisher exact test, *P*-value after Bonferroni correction; n.s., not significant; ****P* < .0001) for the different cell types. **C** Heatmap showing the scaled expression levels of upregulated genes in malignant cells compared to the normal group. The genes are grouped by their functional categories, including cell stemness related, glycolysis, myeloid maturation, and erythroid related. **D** Radar plot showing the Gene Set Variation Analysis (GSVA) scores for selected signal pathways, including stem cell proliferation, differentiation, migration, maintenance of stemness, glycolysis, and oxidative phosphorylation, in normal and malignant HSC/MPPs cells. The plot illustrates the differential enrichment of these stem cell-related pathways between the HSC/MPP-normal and HSC/MPP-malignant cell states. **E** Radar plot showing the GSVA scores for selected signaling pathways, including myeloid cell proliferation, differentiation, activation, leukemia suppressor signaling, glycolysis, and oxidative phosphorylation, in the two cell states of normal and malignant GMPs cells. The plot illustrates the differential enrichment of these myeloid-related pathways between the GMP-normal and GMP-malignant cell states. **F** Inferred activated (red) and repressed (blue) regulatory proteins in malignant cells compared to control group. The arrows indicate the distribution of activated (red) and repressed (blue) targets for different regulatory proteins, with their positions sorted based on the differential expression between malignant group and the control group (leftmost: most upregulated in malignant cells, rightmost: most downregulated in malignant cells). The *P*-values are shown on the left side of each row. **G** Gene regulatory network (GRN) visualization of differentially active regulatory proteins (*ENO1*, *TCF4*, *ID1*, and *SREBF1*) and their target differentially expressed genes (DEGs) in malignant cells

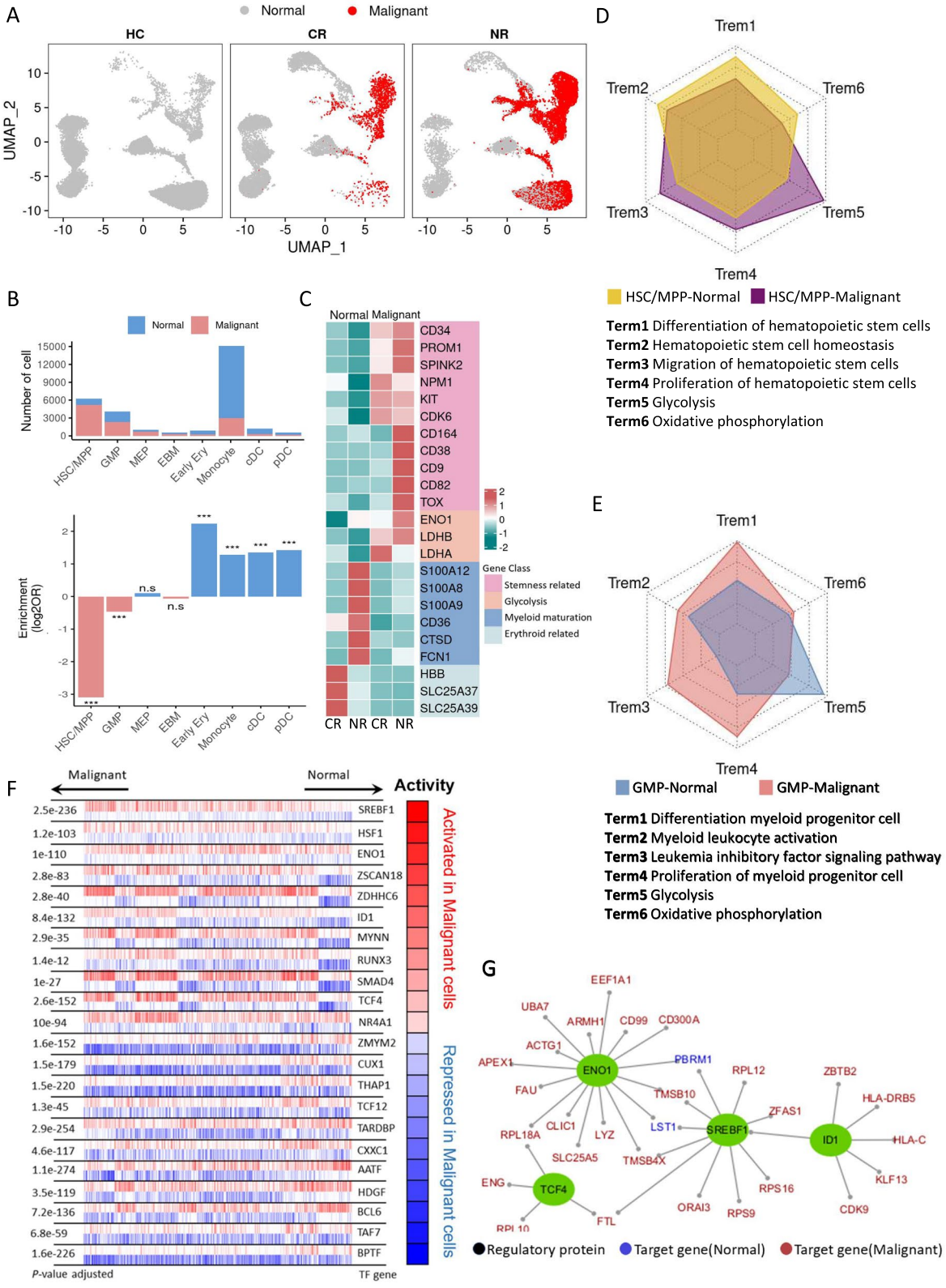

Fig. 2 (See legend on previous page.)

Our analysis showed that the malignant cells by our model, were predominantly composed of primitive progenitor cells or myeloid cells (12,267 cells), with a very small number of predicted mid-to-late-stage erythrocytes (3 cells) and a few T, B, and NK cells (32 cells combined). Further analysis comparing malignant cells (malignant group) with normal hematopoietic lineages cells (normal group) revealed that malignant group predominantly consisted of highly proliferative HSC/MPPs and GMPs populations. In contrast, the normal group exhibited a preference towards more mature myeloid cells such as monocytes, cDCs, pDCs, and early erythrocytes (Fig. 2B; Supplementary Fig. 3B).

To further elucidate gene-level changes, we screened for the DEGs between the malignant and normal groups (Supplementary Table S2). The results showed that, consistent with the cell composition, stemness-related genes were significantly enriched in malignant cells (e.g., *CD34*, *PROM1*, *CD164* and *SPINK2*) (Fig. 2C) [56–58]. Notably, genes considered as LSCs markers, such as *CD9*, *CD82*, and *CDK6*, were upregulated in malignant cells, especially in the NR group [13, 14, 59]. Additionally, genes related to immune cell exhaustion such as *TOX* [60], as well as *CDK6*, *KIT*, and *NPM1*, which were involved in cell proliferation and differentiation, were upregulated in malignant cells and were often associated with poor prognosis in AML patients [61–63]. Furthermore, glycolysis-related genes such as *ENO1*, *LDHB*, and *LDHA* were upregulated in malignant cells, potentially associated with the malignant cells' reprogramming of metabolic pathways to meet the demands of rapid proliferation and to gain advantages through the accumulation of metabolic products [18, 64]. Conversely, myeloid genes regulating inflammation and immune response, such as *S100A12*, *S100A8*, *S100A9*, *CTSD*, *FCN1*, and *CD36*, were downregulated in the malignant cells [65]. In the CR group, the normal cells primarily consisted of erythrocytes, with upregulation of hemoglobin (*HBB*) and mitochondrial hemesynthesis genes (*SLC25A37* and *SLC25A39*) [66].

Next, we conducted GSVA enrichment analysis on the predominant clusters (HSC/MPPs and GMPs) identified as malignant group to compare their functional differences with the normal group (Supplementary Table S3). Compared to the HSC/MPPs in normal group (HSC/MPP-normal), HSC/MPPs in the malignant group (HSC/MPP-malignant) exhibited enhanced proliferative capacity and weaker differentiation ability. They demonstrated increased migratory potential, including stronger homing ability to the BM, but weaker capability to maintain hematopoietic stem cell homeostasis. Consistent with this, HSC/MPP-malignant were enriched with genes related to glycolysis (*ENO1*, *LDHA*, *LDHB*), indicating heightened glycolytic activity while showing slightly OXPHOS capacity (Fig. 2D). Additionally, compared to GMPs cells in the normal group (GMP-normal), GMP cells in AML malignant cells group (GMP-malignant) showed enhanced proliferation and differentiation capabilities, along with heightened activation of myeloid cells and production of leukemia inhibitory factors, suggesting an inflammatory state (Supplementary Table S4). Conversely, the GMP-normal exhibited stronger glycolytic capacity compared to GMP-malignant, while OXPHOS functions were similar between the two groups (Fig. 2E). The significant variations in glycolytic function observed in HSC/MPPs and GMPs cells inversely correlated with their differentiation tendencies.

Finally, we conducted VIPER analysis to elucidate the key regulatory proteins in AML malignant cells that may promote malignant transformation and tumor progression by regulating specific transcriptional networks (Fig. 2F). The results showed that several key regulatory proteins were upregulated in malignant cells compared to normal cells, such as *HSF1* and *ID1*, which drive LSCs self-renewal [67, 68]; *TCF4* and *SMAD4*, which are involved in malignant cells proliferation; *RUNX3*, which inhibits myeloid development and is associated with drug resistance [69, 70]; and *ENO1* and *SREBF1*, which regulate proliferation and metabolism [25, 71]. These key regulators are often associated with poor prognosis (Fig. 2F; Supplementary Fig. 3C). To gain deeper insights into the molecular interactions in AML, we constructed a GRN of differentially expressed genes. Network analysis highlighted hub nodes such as *ENO1*, *SREBF1*, and *TCF4*, whose target genes tended to be upregulated in AML malignant cells, suggesting that the activation of these key regulators may lead to the activation of multiple aberrant signaling and metabolic pathways, thereby promoting AML development and maintenance (Fig. 2G).

ENO1 involvement in differentiation blockage of malignant Cells

Given that one of the pathogenesis mechanisms of AML is the developmental arrest and abnormal proliferation of stem or progenitor cells in the BM, we performed pseudotime analysis on the scRNA-seq data of HSC/MPPs, GMPs, monocytes, and DCs (cDCs and pDCs) cells to further explore the differentiation process involving normal and malignant myeloid cells. The results showed that although normal and malignant cells had similar developmental trajectory patterns, the differentiation boundaries of malignant cells were unclear and were significantly delayed compared to normal cells (Fig. 3A, B, Supplementary Fig. 4A). Specifically, the pseudotime distribution of malignant cells was significantly more biased

towards the early phase of the differentiation trajectory, than the normal cells (*P*-value < 2.2e−16) (Fig. 3B).

Next, we utilized the branching expression analysis modeling (BEAM) method to further investigate the key genes that correlated the differentiation trajectory of normal and malignant cells. We found that *ENO1* was co-expressed with cell stemness related genes (*CD34*, *SPINK2* and *PROM1*) and LSCs specific genes (*CD82* and *CD9*) and was highly expressed in the pre-branch stage of the BEAM heatmap (Fig. 3C). The malignant cells were enriched for genes driving cells towards cell fate 1, whereas genes driving cells to fate 2 were mostly expressed in normal cells (Fig. 3C; Supplementary Fig. 4B). Further, we focused on examining the gene expression levels of *ENO1* in different cell types within the pseudotime series, with particular emphasis on comparing patients in the CR and NR groups (Fig. 3D). We observed that NR patients exhibited significantly higher expression of *ENO1* in the initial stage of the pseudotime, specifically in HSC/MPPs, compared to the CR group. Considering the co-expression of *ENO1* with cell stemness related genes in the BEAM heatmap and its contrasting trends in glycolysis and cell differentiation in HSC/MPP-malignant (LSCs) and GMP-malignant cells, we hypothesized that *ENO1* might be involved in the maintenance of cellular self-renewal, particularly in LSCs.

Comparison of *ENO1* expression levels among different cell types revealed predominant expression in hematopoietic stem/progenitor cells (HSC/MPPs, GMPs), and myeloid lineage cells (monocytes, DCs) (Supplementary Fig. 4C). We then focused on the expression levels of *ENO1* in HSC/MPPs, GMPs, monocytes and DCs under different conditions. In malignant cells, the expression levels of *ENO1* in HSC/MPPs, GMPs, monocytes, and DCs were significantly higher than in normal cells (Fig. 3E). Monocytes from CR patients, which were fewer in number and mostly malignant, exhibited higher *ENO1* expression levels compared to NR patients (Figs. 2A and 3F). However, *ENO1* expression in HSC/MPPs, GMPs, and DCs was significantly lower in CR patients than in NR patients (Fig. 3F). Overall, the expression levels of *ENO1* in NR patients were significantly higher than those in CR patients and HCs (*P*-value < 2.2e−16) (Fig. 3G). We then performed qRT-PCR analysis on peripheral blood samples from 28 newly diagnosed AML patients collected at our center, and compared to samples from 38 healthy individuals. The results showed that *ENO1* expression levels were significantly higher in AML patients compared to HCs (*P*-value = 0.0001) (Fig. 3H left). Furthermore, based on treatment response, CR patients showed significantly lower *ENO1* expression levels compared to NR patients (*P*-value = 0.0006) (Fig. 3H right). More importantly, the 1-year survival rate of high *ENO1* expression patients was only 10.0%, significantly lower than the 59.1% observed in the low expression group (*P*-value = 0.0038) (Fig. 3I; Supplementary Fig. 4D). Thus, these results collectively revealed that high *ENO1* expression is potentially associated with poor prognosis in AML patients, and high *ENO1* expression in malignant cells may play a crucial role in blocking HSC/MPPs cell differentiation.

High expression of *ENO1* in LSCs contributes to self-renewal and chemoresistance

Based on the critical role of *ENO1* in HSC/MPPs, we further analyzed the HSC/MPP cells of AML patients and identified four distinct clusters, designated as HSC/

(See figure on next page.)

Fig. 3 *ENO1* involvement in differentiation blockage of AML malignant Cells. **A** Cell fate trajectory analysis of the four major myeloid cell lineages, including HSC/MPPs, GMPs, monocytes, and DCs. Scatter plots show the distribution of these cell types in normal (left) and malignant (right) samples, where each dot represents a single cell colored by cell type. **B** Comparison of the myeloid differentiation pseudotime (calculated by Monocle) between malignant cells and normal cells using HSC/MPPs as the starting point. Box plot (top) and density plot (bottom) depicting the pseudotime distribution of myeloid differentiation in malignant cells (red) and the normal cells (blue). **C** BEAM heatmap visualization of gene expression levels, where the expression profiles are correlated with the pseudotime trajectory. Proportions of cells mapped to each trajectory branch from the normal and malignant groups are shown underneath the heatmap. **D** Density plot showing the distribution of cells highly expressing *ENO1* across pseudotime for CR (left) and NR (right) patients, with cell types (HSC/MPPs, GMPs, Monocyte, and DCs) indicated by distinct colors. **E** & **F** Violin plots comparing the expression levels of *ENO1* in different cell types (HSC/MPPs, GMPs, Monocyte, and DCs) between CR and NR conditions (**E**) and between malignant and the normal cells (**F**). For the embedded boxplots, the bottom and top of the box are located at the 25th and 75th percentiles, respectively. The bars represent values more than 1.5 times the interquartile range from the border of each box. The same applies to the rest of paper. The *P*-values were calculated using the Wilcoxon rank-sum test (two-sided; ****$P < 0.0001$, ***$P < 0.001$, **$P < 0.01$, *$P < 0.05$, ns: not significant). **G.** Violin plot showing the *ENO1* expression levels in HC (blue), CR (pink), and NR (purple) groups. The bottom and top of the box are located at the 25th and 75th percentiles, respectively. The Kruskal–Wallis test ($P < 2.2e\text{-}16$) indicates a significant difference among the groups. **H** Beeswarm plots comparing the differences in *ENO1* mRNA expression levels measured by qPCR between HCs and AML patients (left panel), as well as between CR and NR patients (right panel). The *P*-values from t-tests indicate that there are significant differences in both comparisons ($P < 0.0001$ and $P = 0.0006$). **I** Survival curves stratifying the AML patients into two groups based on the optimal cut-off value, showing that the high *ENO1* expression group had significantly poorer prognosis compared to the low expression group (Log-rank test, $P = 0.0038$)

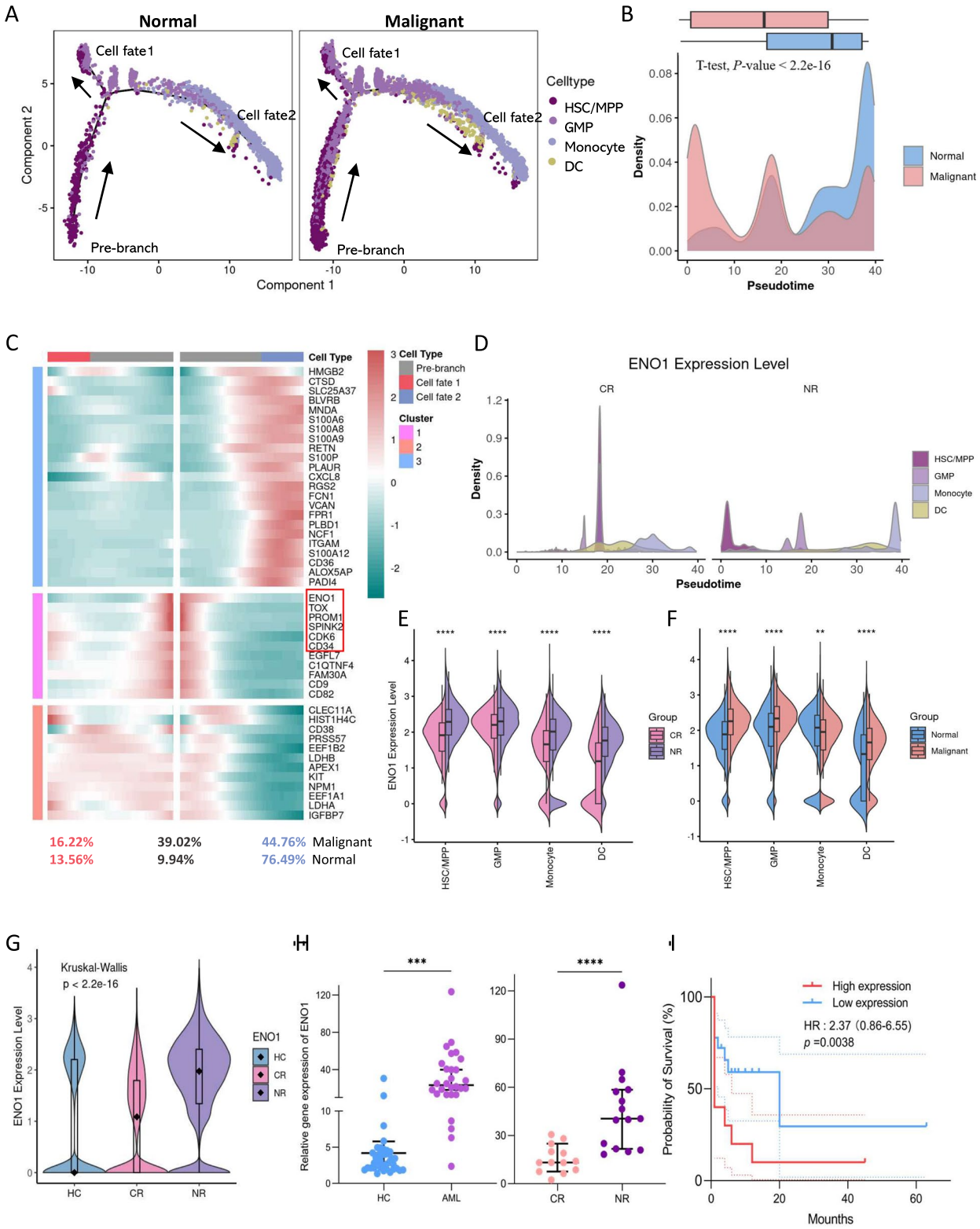

Fig. 3 (See legend on previous page.)

MPP-1, HSC/MPP-2, HSC/MPP-3, and HSC/MPP-4 (Fig. 4A). Through comparative analysis, we observed that HSC/MPP-1, HSC/MPP-2, and HSC/MPP-3 were predominantly composed of malignant cells, with the majority originating from patients in the NR group (Fig. 4B, C; Supplementary Fig. 5A, B). We then compared the functional and regulatory characteristics of the four clusters by calculating DEGs and conducting functional scoring (Supplementary Table S5). The analyses indicated that HSC/MPP-1 upregulated several *ENO1* target genes, such as *CD300A* and *TMSB10*, exhibiting the highest stemness score; HSC/MPP-2 upregulated more chemotaxis-related genes like *CXCL2*, *CXCL3*, and *CXCL8* [72], showing the highest chemotaxis and differentiation scores; HSC/MPP-3 upregulated proliferation-related genes such as *STMN1*, *TYMS*, and *CDCA7*, displaying the highest proliferation score; the HSC/MPP-4 cluster, primarily from the CR group, upregulated several long non-coding RNAs, such as *SNHG29*, *GAS5*, *SNHG6*, and *SNHG5* (Fig. 4D, E).

Next, we inferred the differentiation order of the predominantly malignant cell clusters (HSC/MPP-1, HSC/MPP-2, and HSC/MPP-3), and discovered that differentiation initiated from the HSC/MPP-1 cluster and progressed towards HSC/MPP-2 and HSC/MPP-3 (Fig. 4F). Observing the expression of *ENO1* within the HSC/MPP clusters, we found the highest expression was in HSC/MPP-1, the cluster with the strongest stemness and mostly identified in the NR patients (Fig. 4G).

Subsequently, we examined the impact of treatment on HSC/MPP cells by integrating them before and after treatment and confirming their consistency with respect to upregulated gene expression (Fig. 4H; Supplementary Fig. 5C). Chemotherapy was more effective in eliminating rapidly proliferating cells, resulting in a significant reduction in the number of cells in the HSC/MPP-3 cluster, which exhibited the strongest proliferative capacity, as well as a notable decrease in the number of cells in the HSC/MPP-4 cluster derived from the CR group (Fig. 4H). On the other hand, there was a significant increase in the number of cells in the HSC/MPP-1 cluster, characterized by the highest expression levels of *ENO1*, and a marked elevation in *ENO1* expression within the HSC/MPP-1 cluster post-treatment (Fig. 4I, J).

Thus, these results collectively showed that the HSC/MPP-1 cluster was composed entirely of cells from the NR group, and based on pseudotime inference, it was postulated to be the origin of malignant stem cells. After treatment, there was a significant increase in the number of cells in this cluster, coinciding with a notable increase in *ENO1* expression levels, suggesting that this cluster continuously maintained self-renewal ability and potentially contributed to chemoresistance.

Downregulating *ENO1* reduces AML cell proliferation and induces differentiation

To further elucidate the functional role of *ENO1* in AML, we constructed a stable knock-down cell line of *ENO1* in MOLM-13 cells by lentivirus transduction. Both WB and qRT-PCR results indicated effective knockdown of *ENO1* expression in the MOLM-13 cell lines (Figs. 5A, B). The CCK-8 assay results showed a reduction in proliferation upon *ENO1* knockdown, with shRNA2 exhibiting the most significant decrease (P-value < 0.0001) (Fig. 5C).

To investigate the regulatory effects of *ENO1* knockdown on MOLM-13 cells and the potential mechanism, transcriptome sequencing was performed on MOLM-13 cells with stable *ENO1* knockdown (*ENO1*_KD). The results revealed that, compared to the control group, a total of 482 differentially expressed genes were identified after *ENO1*_KD, with 127 genes upregulated and 355 genes downregulated (|Log2FC| > 1 and P-value < 0.05) (Fig. 5D). We used GSVA to assesses the functional differences of MOLM-13 cells after *ENO1*_KD (Supplementary Table S6). The results demonstrated the upregulated genes after *ENO1*_KD were enriched for GO terms

(See figure on next page.)

Fig. 4 High expression of *ENO1* promotes self-renewal and chemoresistance of LSCs. **A** UMAP plot showing the distribution of HSC/MPP subpopulations (HSC/MPP-1, HSC/MPP-2, HSC/MPP-3, HSC/MPP-4) in the dataset. Each subpopulation is color-coded as indicated. **B** UMAP plot showing the distribution of malignant cells (red) and normal cells (gray) among the HSC/MPP cells. **C** Bar plot showing the proportion of each HSC/MPP subpopulation in HC, CR, and NR. Each condition is color-coded as indicated. **D** Heatmap showing the expression levels of DEGs across HSC/MPP subpopulations. Each column represents a cell, and each row represents a gene. The color scale indicates relative expression levels. **E.** Violin plots comparing the stemness, differentiation, proliferation, and chemotaxis scores across HSC/MPP subpopulations (HSC/MPP-1, HSC/MPP-2, HSC/MPP-3 and HSC/MPP-4). **F** UMAP plots showing the cell fate trajectory of HSC/MPP-1, HSC/MPP-2, and HSC/MPP-3, primarily composed of malignant cells, with cell clusters information mapping (top) and pseudotime inferred by Monocle3 (bottom). **G** UMAP plots showing the expression levels of *ENO1* in HSC/MPP split by different groups (HC, CR, and NR). Color intensity represents expression level, with deeper colors indicating higher expression levels. **H** UMAP plots showing the distribution of HSC/MPP subpopulations before and after treatment. Subpopulations are color-coded as indicated. **I** Bar chart showing the abundance of each HSC/MPP cell subtype before (purple) and after (yellow) treatment. **J** Violin plots comparing *ENO1* expression levels in HSC/MPP subpopulations before (purple) and after (yellow) treatment. The P-values were calculated using the Wilcoxon rank-sum test (two-sided; ****P < 0.0001, ***P < 0.001, **P < 0.01, *P < 0.05, ns: not significant)

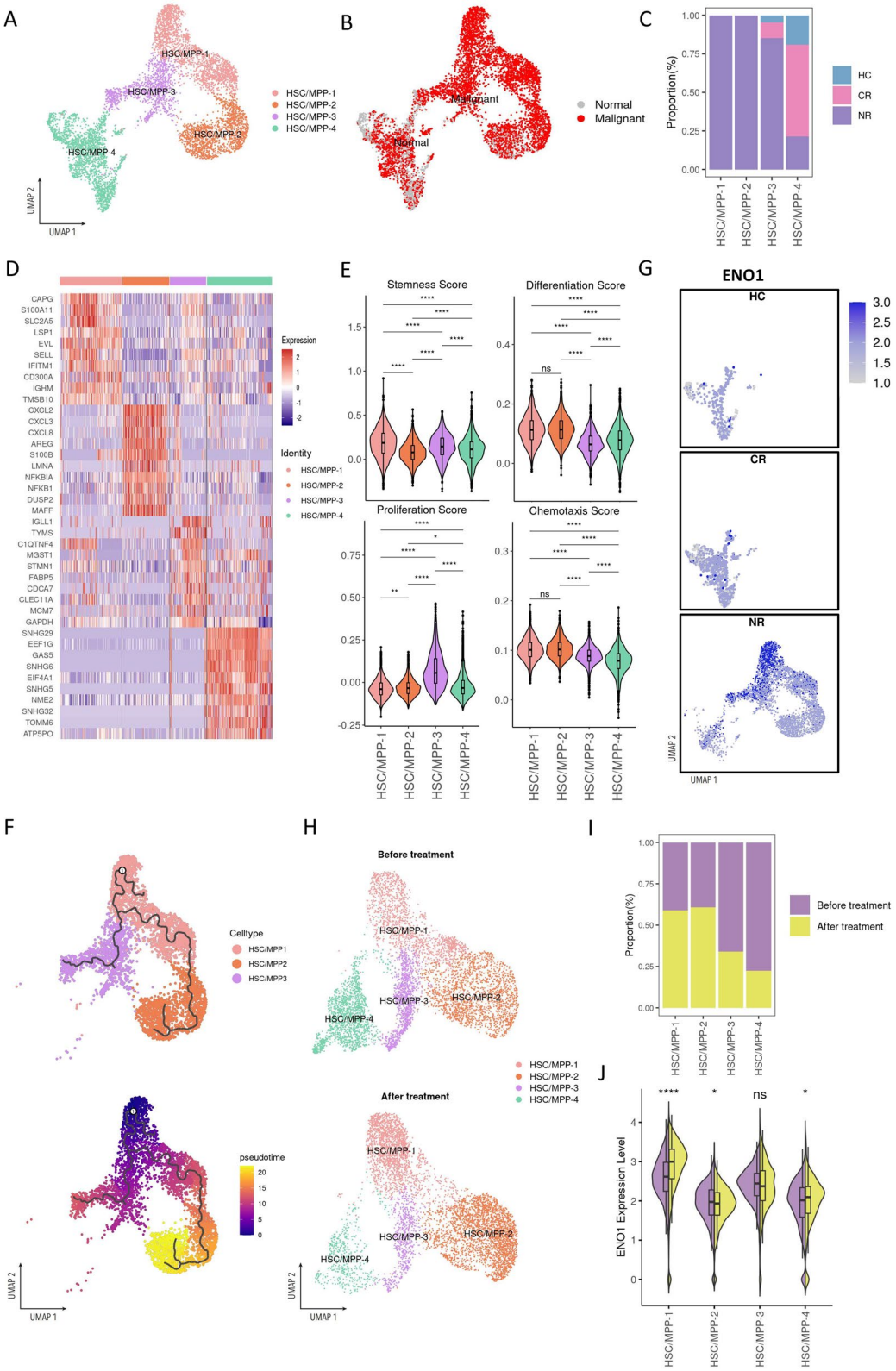

Fig. 4 (See legend on previous page.)

associated with hematopoietic stem cell differentiation and myeloid cell apoptotic processes (Fig. 5E). In contrast, the downregulated genes in *ENO1*_KD were primarily enriched for functions related to hematopoietic stem cell and myeloid progenitor cell proliferation. These findings suggest that *ENO1*_KD may promote LSCs differentiation while inhibiting their proliferation.

The activation and quiescence states of LSCs are closely associated with the treatment of AML. It is generally believed that quiescent LSCs are more prone to immune evasion, chemotherapy resistance, and disease relapse, while activation LSCs tend to undergo cellular differentiation. Thus, we assessed the quiescence and activation scores of MOLM-13 cells before and after *ENO1*_KD using a dataset (Supplementary Table S7) [54]. *ENO1*_KD disrupted the balance between LT-HSC activation and quiescence. Following knockdown, there was a significant increase in the activation scores of LT-HSC, suggesting that *ENO1* may play a role in maintaining LSCs in a quiescent state (Fig. 5F).

Since *ENO1* has been implicated in poor prognosis of AML, we further investigated the effects of *ENO1* functional inhibition on AML cell line. We treated MOLM-13 cells with the *ENO1* inhibitor AP3-III-a4. The results showed that AP3-III-a4 inhibited the proliferation of MOLM-13 cells in a time and dose dependent manner (Fig. 5G). This finding suggests that targeting *ENO1* may represent a valid therapeutic strategy for eliminating LSCs and improving the treatment outcomes of AML.

Discussion

ENO1 has been shown to play a crucial role in the occurrence, development, and metastasis of numerous types of tumors, suggesting its potential as an oncogene [23, 25]. In the digestive system, overexpression of *ENO1* has been associated with poor clinical outcomes in gastric cancer, hepatocellular carcinoma, pancreatic cancer, and colorectal cancer [73–76]. In the respiratory system, *ENO1* promotes the self-renewal and malignant phenotype of lung cancer stem cells through the AMPK/mTOR pathway [77]. Furthermore, the serum levels of anti-ENO1 autoantibodies are related to the clinical staging of lung cancer, with significantly higher levels observed in Stage I and II patients compared to Stage III and IV patients (P-value < 0.01) [78]. Decreased serum ENO1 antibodies serve as markers for advanced breast cancer [79]. Furthermore, inhibition of *ENO1* has been found to suppress the proliferation of retinoblastoma [80]. In head and neck cancer, *ENO1* expression stimulates cell transformation, invasion, and tongue tumor formation [81]. In hematologic malignancies, compared to healthy controls, elevated expression of *ENO1* and lower levels of circulating anti-ENO1 autoantibodies have been observed in patients with myelodysplastic syndromes and AML [28, 82]. However, the functional role and underlying mechanisms of ENO1 in AML remain unclear. To gain a comprehensive understanding of the biological significance and clinical implications behind this phenomenon, it is essential to focus research efforts at the cellular level. In this study, we integrate single-cell data with machine learning techniques to model and infer malignant cell population in AML at a higher resolution. We found that *ENO1* is involved in maintaining the self-renewal of LSCs and contributes to chemotherapy resistance. Knocking down *ENO1* resulted in a decrease in LSCs proliferation and promoted differentiation.

LSCs play a major role in the initiation, progression, and relapse of AML [83, 84]. They possess the capacity to initiate the disease, hence they are also referred to as "leukemia-initiating cells" (LICs) [85]. Additionally, LSCs can switch to a quiescent state to evade the effects of chemotherapy, which often renders them resistant to chemotherapeutics and may result in relapse [84–86]. Therefore, the quiescent state of LSCs makes the treatment of AML particularly challenging. This means that targeted therapy for the quiescent state of LSCs may be a potential strategy to enhance the effectiveness of AML treatment and improve long-term survival rate of AML

(See figure on next page.)

Fig. 5 Impact of *ENO1* knockdown on leukemic cell survival and apoptosis. **A** Western blot results showing *ENO1* protein levels in MOLM-13 cells transduced with control shRNA or three different *ENO1*-targeting shRNAs (shRNA1, shRNA2 and shRNA3). β-Actin served as a loading control. **B** Bar graph depicting the relative expression levels of *ENO1* mRNA in MOLM-13 cells transducted with control shRNA or *ENO1*-targeting shRNAs (shRNA1, shRNA2 and shRNA3), measured by qPCR. ***$P < 0.001$. **C** Line graph showing the cellular viability of MOLM-13 cells transducted with control shRNA or *ENO1*-targeting shRNAs (shRNA1, shRNA2 and shRNA3) after 72 hours, as measured by OD450. Error bars in bar plots represent the means ± SE. P-values was calculated using Wilcoxon test (two-sided; ****$P < 0.0001$, ***$P < 0.001$, **$P < 0.01$, *$P < 0.05$, ns: not significant). **D** Line plot (left panel) and heatmap (right panel) showing the clustering of DEGs in MOLM-13 cells with *ENO1* knockdown (*ENO1*_KD) compared to the control group, as analyzed by RNA-seq. Gene symbols of selected genes with significant alteration are shown. **E** Heatmap of GSVA scores of shared and specific GO terms enriched for *ENO1*_KD and control group. **F** Scatter plot showing the activation and quiescence scores of long-term hematopoietic stem cells (LT-HSCs) in the *ENO1*_KD group and control group. **G** Line graph illustrating the cellular viability of MOLM-13 cells after treatment with different concentrations of an *ENO1*-inhibitor (AP3-III-a4) for different time, as assessed by OD450. Statistical significance was determined by one-way ANOVA (****$P < 0.0001$)

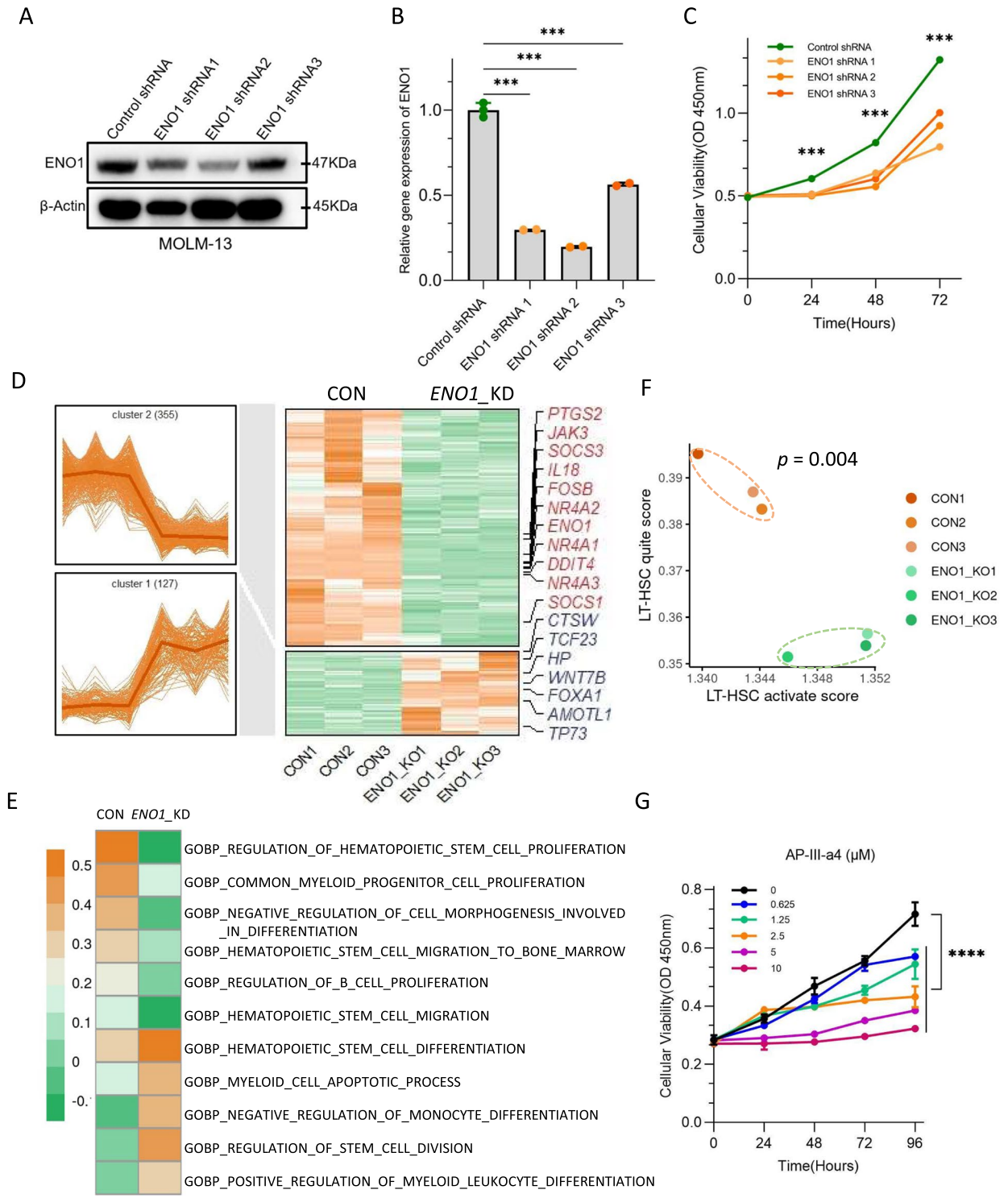

Fig. 5 (See legend on previous page.)

patients. Our results showed that in AML patients, the predominant cells are stem and progenitor cells, most of which are malignant cells, especially in NR patients. The abundance of these cells may influence the patients' ability to respond to treatment. AML malignant cells upregulate stem cell-related genes such as *CD34* and *PROM1* [56–58], which are highly expressed in AML patients. Notably, LSCs marker genes such as *CD9* and

CD82 are upregulated in malignant cells [13, 14], especially in the NR group, supporting the accuracy of our predictions. By comparing the dominant HSC/MPP and GMP cells in malignant cells with normal cells, we find that although HSC/MPP-malignant and GMP-malignant cells exhibit greater proliferative capacity, their differentiation ability and glycolysis show an inverse relationship. Specifically, HSC/MPP-malignant cells have significantly weaker differentiation ability than HSC/MPP-normal cells, yet stronger glycolysis. Conversely, malignant GMP-malignant cells have stronger differentiation ability but weaker glycolytic function compared to GMP-normal cells. This indicates that glycolysis and related genes or products in its metabolic pathway play a regulatory role in cell differentiation.

Our analysis revealed the upregulation of several key regulatory proteins in malignant cells. In addition to proteins associated with the self-renewal of LSCs (*HSF1* and *ID1*) [67, 68] and the proliferation of leukemia cells (*TCF4* and *SMAD4*) [69, 70], *ENO1* was found to be more active in malignant cells, with its regulated genes also upregulated in these cells. Pseudotime analysis showed that *ENO1* was co-expressed with stem cell-related genes (*CD34*, *PROM1*) [56–58] and LSC-specific genes (*CD9*, *CD82*) [13, 14] and was present at the early differentiation stage. During the maturation of myeloid cells in pseudotime, there was a significant difference in *ENO1* expression in HSC/MPPs between the NR and CR groups. Further analysis of the HSC/MPPs cluster revealed that the HSC/MPP-1 subtype, characterized by high *ENO1* expression, originated solely from NR patients and was at an early differentiation stage. After treatment, the number of HSC/MPP-1 subtype cells significantly increased, with markedly elevated *ENO1* expression, whereas the number of the more proliferative HSC/MPP-3 subgroup and the HSC/MPP-4 subgroup primarily from CR patients significantly decreased. This indicates that the HSC/MPP-1 subtype with high *ENO1* expression maintains self-renewal during chemotherapy, potentially being a key factor in chemoresistance in NR patients.

High *ENO1* expression in AML is not only associated with differentiation blockade but also with poor patient prognosis. The clinical samples at our center revealed that *ENO1* expression was significantly higher in AML patients than in healthy, particularly in NR patients. Moreover, the AML patients with high *ENO1* expression had significantly shorter survival times than those with low expression. This finding is consistent with recent results from Lincz et al., who conducted an integrated analysis of nine online AML datasets ($n=1,419$ patients) and found that high *ENO1* expression predicts poor overall survival [28]. We further validated the critical role of *ENO1* in AML cells. Knocking down the *ENO1* gene significantly reduced AML cell proliferation and promoted their differentiation. Further, after knocking down *ENO1*, AML cells were significantly enriched in genes related to HSC differentiation, myeloid cell differentiation, and apoptosis, tending to activate LT-HSC. The *ENO1* inhibitor treatment also significantly suppressed AML cell proliferation. These results suggested that targeting *ENO1* may represent a potential therapeutic strategy to inhibit LSC self-renewal and improve the treatment outcomes of AML. While measuring *ENO1* could be recommended as a biomarker for monitoring AML prognosis.

Our study has some limitations. Firstly, there is a need to enhance the depth of mechanism. Although our results indicate the involvement of *ENO1* in regulating LSC function, the specific molecular mechanisms have not been thoroughly investigated. Future studies should integrate methods such as proteomics and metabolomics, along with relevant experiments, to provide a deeper understanding of the molecular mechanisms by which *ENO1* regulates AML development. Secondly, it is important to explore optimal drug combinations. Combining chemotherapy drugs with *ENO1* inhibitors may contribute to more effective LSCs elimination and improving patient prognosis. Further research and clinical trials are essential to investigate the synergistic effects of combining *ENO1* inhibitors with conventional chemotherapy drugs, aiming to provide enhanced therapeutic outcomes for AML patients.

Conclusions

The present study highlights the significant role of *ENO1* in the proliferation, differentiation, and treatment resistance of LSCs. Targeting *ENO1* may represent a promising therapeutic strategy for eliminating LSCs and improving the clinical prognosis of AML patients.

Abbreviations

AML	Acute myeloid leukemia
HSCT	Hematopoietic stem cell transplantation
LSCs	Leukemia stem cells
HSCs	Hematopoietic stem cells
OXPHOS	Oxidative phosphorylation
ENO1	Alpha-enolase
R/R AML	Relapsed/refractory AML
2-PG	2-Phosphoglycerate
PEP	Phosphoenolpyruvate
CR	Complete remission
NR	Non-response
HCs	Healthy controls
scRNA-seq	Single-cell RNA sequencing
CNVs	Copy number variations
BM	Bone marrow
HSC/MPPs	Hematopoietic stem cells/multipotent progenitors
GMPs	Granulocyte-monocyte progenitors
MEPs	Megakaryocyte-erythroid progenitors
EBMs	Eosinophil, basophil, and mast cell progenitors
Erys	Erythrocytes
NK	Natural killer

cDCs	Conventional dendritic cells
pDCs	Plasmacytoid dendritic cells
DEGs	Differentially expressed genes
GO	Gene ontology
GSVA	Gene set variation analysis
VIPER	Virtual inference of protein-activity by enriched regulon analysis
GRN	Gene regulatory network
BEAM	Branching expression analysis modeling
qRT-PCR	Quantitative reverse transcription polymerase chain reaction
ROC	Receiver operating characteristic
AUC	Area under the curve
CCK8	Cell Counting Kit-8
WB	Western blotting
shRNA	Short hairpin RNA
LT-HSC	Long-term hematopoietic stem cell
LICs	Leukemia-initiating cells

Supplementary Information

The online version contains supplementary material available at https://doi.org/10.1186/s13287-024-03969-w.

Supplemental Figure 1: UMAP visualization of scRNA-seq data of all samples for cell population distribution and marker gene projection. **A.** UMAP plots of scRNA-seq data from acute myeloid leukemia patients and healthy controls (HCs). Each panel represents a different sample, with dots colored by condition: HCs (blue), complete remission (CR, pink), and non-response (NR, purple). The UMAP projections show the distribution and clustering of cells, revealing distinctions between AML patients and HCs. **B.** Projection of expression of selected marker genes on UMAP plots. The color gradient indicates the gene expression intensity, highlighting the presence and distribution of specific cell populations within the UMAP space. Supplemental Figure 2: Analysis of cell type composition in AML patients and HCs. **A.** UMAP plots displaying the distribution of various cell types in AML (left) and HCs (right). Each cell type is color-coded as indicated in the legend. This visualization shows the distinct clustering patterns and differences in cellular composition between AML patients and healthy controls. **B.** Stacked bar plot showing the relative percentages of different cell types in each sample. The clusters include hematopoietic stem cells/multipotent progenitors (HSC/MPPs), granulocyte-monocyte progenitors (GMPs), megakaryocyte-erythroid progenitors (MEPs), eosinophil, basophil, and mast cell progenitors (EBMs), erythrocytes (early, mid, and later Erys), monocytes, B cells, T cells, natural killer (NK) cells, conventional dendritic cells (cDCs), and plasmacytoid dendritic cells (pDCs). The x-axis represents the individual samples, while the y-axis shows the cumulative proportion of the cell types. Supplemental Figure 3: Identification of malignant cells and their regulatory proteins in AML. **A.** Receiver operating characteristic (ROC) curve showing the performance of the classification model in distinguishing malignant cells from normal cells, with an area under the curve (AUC) of 0.99. **B.** Bar plot displaying the proportion of malignant cells (red) and normal cells (gray) in each cell type, highlighting the differences in the distribution of malignant and normal cells across different cell types. **C.** Kaplan-Meier survival curves for overall survival in AML patients stratified by gene expression levels. Kaplan-Meier plots showing the overall survival of AML patients with low (red) and high (blue) expression levels of the following genes: *SREBF1*, *MYNN*, *RUNX3*, *ENO1*, *ZDHHC6*, *ZSCAN18*, *TCF4*, *HSF1*, and *ID1*. Each plot provides the log-rank p-value and hazard ratio (HR) with 95% confidence intervals. Supplemental Figure 4: *ENO1* expression across different hematopoietic cell types. **A.** Visualization of the cell trajectory for the normal (left) and malignant (right) cells with pseudotime information mapping. Each point represents a single cell, with dark blue indicating the start of differentiation and light blue indicating the end of differentiation. **B.** Heatmap showing the average expression levels of the differentially expressed genes in normal and malignant cells. **C.** Violin plot illustrating the expression levels of *ENO1* across different cell types, including HSC/MPPs, GMPs, MEPs, EBMs, Early Erys, Mid Erys, Later Erys, Monocytes, cDCs, pDCs, B, T, and NK cells. The black diamonds represent the median expression levels for each cell type. **D.** ROC curve generated based on the *ENO1* mRNA expression levels in AML patients to predict classification. The optimal cut-off value was determined to be 35.12 cycle, with an AUC of 0.9182 ($P = 0.0002$), indicating good accuracy in distinguishing high *ENO1* expressers from low *ENO1* expressers among the AML samples. Supplemental Figure 5: Analysis of hematopoietic stem cell and progenitor cells in different conditions. **A.** UMAP plots illustrating the distribution of HSC/MPP subpopulationsin HC, CR, and NR. Each subpopulation is color-coded as indicated. **B.** Bar chart showing the proportions of each cell type in malignant cells (red) and normal cells (gray), highlighting the distribution differences of malignant and normal cells among HSC/MPP subpopulations. **C.** Heatmap showing the expression levels of differentially expressed genes in HSC/MPP subpopulations from after treatment samples. Each column represents a cell, and each row represents a gene. The color scale indicates the relative expression levels.

Acknowledgements
We thank Department of Hematology, First Affiliated Hospital, Jinan University, for providing samples for validation. The authors declare that they have not used Artificial Intelligence in this study.

Author contributions
YT performed sequencing data analysis, conducted parts of the experiment and wrote the paper. JG and ZC collected samples, conducted part of the experiment. LM assisted with the data interpretation and wrote the paper. XZ collected samples. YL, XZ, YZ and OL conceived the study, designed the experiments, and oversaw the research project. All authors contributed to the article and approved the submitted version.

Funding
This study was supported by grants from the National Natural Science Foundation of China (82350610280, 92370107, 82293632 and 82400259); the Guangdong Basic and Applied Basic Research Foundation (2024A1515011034); the China Postdoctoral Science Foundation (2021M701427 and 2013M540685); the Pearl River Talents Scheme of Guangdong Province (2019QN01Y990). O. J. L. gratefully acknowledges the support of K. C. Wong Education Foundation.

Availability of data and materials
The bulk RNA-seq data from AML cell line (MOLM-13) analyzed in this study are available through Zenodo at https://zenodo.org/records/13831207. The scRNA-seq data are collected from published studies, with data of 8 R/R AML patients sourced from GSE223844 and data of 4 healthy donors obtained from GSE116256 of the GEO database (Gene Expression Omnibus, https://www.ncbi.nlm.nih.gov/geo/).

Declarations

Ethics approval and consent to participate
This study was approved by the Ethics Committee of the School of Medicine, Jinan University (Approval No. [2015] Ethics Approval Section 009). Title of the approved project: Reversal Regulation of TCR VβT Cell Clone Dysfunction Mediated by Immune Checkpoint Receptors in AML. Date of approval: 01 January, 2016.

Consent for publication
The consent for publication was acquired from patients/participants. All authors confirm their consent for publication.

Competing interests
The authors declare that they have no competing interests.

Author details
[1]Key Laboratory for Regenerative Medicine of Ministry of Education, Institute of Hematology, Jinan University, Guangzhou 510632, China. [2]Department of Hematology, First Affiliated Hospital of Jinan University, Guangzhou 510632, China. [3]Department of Systems Biomedical Sciences, School of Medicine, Jinan University, Guangzhou 510632, China. [4]Department of Clinical Laboratory, First Affiliated Hospital of Jinan University, Guangzhou 510632, China. [5]Guangdong Provincial Key Laboratory of Spine and Spinal Cord

Reconstruction, The Fifth Affiliated Hospital of Jinan University (Heyuan Shenhe People's Hospital), Jinan University, Heyuan 517000, China.

Received: 31 July 2024 Accepted: 30 September 2024
Published online: 08 October 2024

References

1. van Galen P, Hovestadt V, Wadsworth Ii MH, Hughes TK, Griffin GK, Battaglia S, et al. Single-cell RNA-seq reveals AML hierarchies relevant to disease progression and immunity. Cell. 2019;176(6):1265-81.e24.
2. Döhner H, Weisdorf DJ, Bloomfield CD. Acute myeloid Leukemia. N Engl J Med. 2015;373(12):1136–52.
3. Mohty R, El Hamed R, Brissot E, Bazarbachi A, Mohty M. New drugs before, during, and after hematopoietic stem cell transplantation for patients with acute myeloid leukemia. Haematologica. 2023;108(2):321–41.
4. Tian C, Chen Z. Immune therapy: a new therapy for acute myeloid leukemia. Blood Sci. 2023;5(1):15–24.
5. DeWolf S, Tallman MS. How I treat relapsed or refractory AML. Blood. 2020;136(9):1023–32.
6. Gudgin EJ, Huntly BJ. Acute myeloid leukemia: leukemia stem cells write a prognostic signature. Stem Cell Res Ther. 2011;2(2):21.
7. Xu C, Lu T, Lv X, Cheng T, Cheng H. Role of the bone marrow vascular niche in chemotherapy for MLL-AF9-induced acute myeloid leukemia. Blood Sci. 2023;5(2):92–100.
8. Thomas D, Majeti R. Biology and relevance of human acute myeloid leukemia stem cells. Blood. 2017;129(12):1577–85.
9. Stelmach P, Trumpp A. Leukemic stem cells and therapy resistance in acute myeloid leukemia. Haematologica. 2023;108(2):353–66.
10. Lapidot T, Sirard C, Vormoor J, Murdoch B, Hoang T, Caceres-Cortes J, et al. A cell initiating human acute myeloid leukaemia after transplantation into SCID mice. Nature. 1994;367(6464):645–8.
11. Jordan CT. Targeting myeloid leukemia stem cells. Sci Transl Med. 2010;2(31):31ps21.
12. Jan M, Chao MP, Cha AC, Alizadeh AA, Gentles AJ, Weissman IL, et al. Prospective separation of normal and leukemic stem cells based on differential expression of TIM3, a human acute myeloid leukemia stem cell marker. Proc Natl Acad Sci U S A. 2011;108(12):5009–14.
13. Marjon KD, Termini CM, Karlen KL, Saito-Reis C, Soria CE, Lidke KA, et al. Tetraspanin CD82 regulates bone marrow homing of acute myeloid leukemia by modulating the molecular organization of N-cadherin. Oncogene. 2016;35(31):4132–40.
14. Liu Y, Wang G, Zhang J, Chen X, Xu H, Heng G, et al. CD9, a potential leukemia stem cell marker, regulates drug resistance and leukemia development in acute myeloid leukemia. Stem Cell Res Ther. 2021;12:1–13.
15. Nagare RP, Sneha S, Priya SK, Ganesan TS. Cancer stem cells - are surface markers alone sufficient? Curr Stem Cell Res Ther. 2017;12(1):37–44.
16. Kreso A, Dick JE. Evolution of the cancer stem cell model. Cell Stem Cell. 2014;14(3):275–91.
17. Mesbahi Y, Trahair TN, Lock RB, Connerty P. Exploring the metabolic landscape of AML: from haematopoietic stem cells to myeloblasts and leukaemic stem cells. Front Oncol. 2022;12:807266.
18. Chelakkot C, Chelakkot VS, Shin Y, Song K. Modulating glycolysis to improve cancer therapy. Int J Mol Sci. 2023;24(3):2606.
19. Intlekofer AM, Finley LWS. Metabolic signatures of cancer cells and stem cells. Nat Metab. 2019;1(2):177–88.
20. Vijayakumar SN, Sethuraman S, Krishnan UM. Metabolic pathways in cancers: key targets and implications in cancer therapy. RSC Adv. 2015;5(52):41751–62.
21. Huppertz I, Perez-Perri JI, Mantas P, Sekaran T, Schwarzl T, Russo F, et al. Riboregulation of Enolase 1 activity controls glycolysis and embryonic stem cell differentiation. Mol Cell. 2022;82(14):2666-80.e11.
22. De Miguel M, Alcaina Y, Sainz de la Maza D, Lopez-Iglesias P. Cell metabolism under microenvironmental low oxygen tension levels in stemness, proliferation and pluripotency. Curr Mol Med. 2015;15(4):343–59.
23. Qiao G, Wu A, Chen X, Tian Y, Lin X. Enolase 1, a moonlighting protein, as a potential target for cancer treatment. Int J Biol Sci. 2021;17(14):3981–92.
24. Chen ML, Yuan TT, Chuang CF, Huang YT, Chung I, Huang WC. A novel enolase-1 antibody targets multiple interacting players in the tumor microenvironment of advanced prostate cancer. Mol Cancer Ther. 2022;21(8):1337–47.
25. Huang CK, Sun Y, Lv L, Ping Y. ENO1 and cancer. Mol Ther Oncolytics. 2022;24:288–98.
26. Zhang T, Sun L, Hao Y, Suo C, Shen S, Wei H, et al. ENO1 suppresses cancer cell ferroptosis by degrading the mRNA of iron regulatory protein 1. Nat Cancer. 2022;3(1):75–89.
27. Kumar KV, Kumar A, Kundal K, Sengupta A, Kunjulakshmi R, Nishana M, et al. AMLdb: A comprehensive multi-omics platform to understand the pathogenesis and discover biomarkers for acute myeloid leukemia. bioRxiv. 2023:2023.05. 19.541403.
28. Lincz LF, Theron DZ, Barry DL, Scorgie FE, Sillar J, Sefhore O, et al. High expression of ENO1 and low levels of circulating anti-ENO1 autoantibodies in patients with myelodysplastic neoplasms and acute myeloid leukaemia. Cancers (Basel). 2024;16(5):884.
29. Zhang W, Liu B, Wu S, Zhao L. TMT-based comprehensive proteomic profiling identifies serum prognostic signatures of acute myeloid leukemia. Open Med (Wars). 2023;18(1):20220602.
30. Zhang Z, Huang J, Zhang Z, Shen H, Tang X, Wu D, et al. Application of omics in the diagnosis, prognosis, and treatment of acute myeloid leukemia. Biomark Res. 2024;12(1):60.
31. Cabello-Aguilar S, Vendrell JA, Van Goethem C, Brousse M, Gozé C, Frantz L, et al. ifCNV: a novel isolation-forest-based package to detect copy-number variations from various targeted NGS datasets. Mol Ther Nucleic Acids. 2022;30:174–83.
32. Gao R, Bai S, Henderson YC, Lin Y, Schalck A, Yan Y, et al. Delineating copy number and clonal substructure in human tumors from single-cell transcriptomes. Nat Biotechnol. 2021;39(5):599–608.
33. Dohmen J, Baranovskii A, Ronen J, Uyar B, Franke V, Akalin A. Identifying tumor cells at the single-cell level using machine learning. Genome Biol. 2022;23(1):123.
34. Warner JK, Wang JC, Hope KJ, Jin L, Dick JE. Concepts of human leukemic development. Oncogene. 2004;23(43):7164–77.
35. Markossian S, Arnaoutov A, Saba NS, Larionov V, Dasso M. Quantitative assessment of chromosome instability induced through chemical disruption of mitotic progression. Cell Cycle. 2016;15(13):1706–14.
36. Eckardt JN, Bornhäuser M, Wendt K, Middeke JM. Application of machine learning in the management of acute myeloid leukemia: current practice and future prospects. Blood Adv. 2020;4(23):6077–85.
37. Schmittgen TD, Zakrajsek BA, Mills AG, Gorn V, Singer MJ, Reed MW. Quantitative reverse transcription-polymerase chain reaction to study mRNA decay: comparison of endpoint and real-time methods. Anal Biochem. 2000;285(2):194–204.
38. Kurien BT, Scofield RH. Western blotting. Methods. 2006;38(4):283–93.
39. Zhang Y, Wu J, Zeng C, Xu L, Wei W, Li Y. The role of NFAT2/miR-20a-5p signaling pathway in the regulation of CD8+ naïve T cells activation and differentiation. Immunobiology. 2021;226(4):152111.
40. Rafat A, Dizaji Asl K, Mazloumi Z, Movassaghpour AA, Talebi M, Shanehbandi D, et al. Telomerase inhibition on acute myeloid leukemia stem cell induced apoptosis with both intrinsic and extrinsic pathways. Life Sci. 2022;295:120402.
41. Bagheri Y, Barati A, Nouraei S, Jalili Namini N, Bakhshi M, Fathi E, et al. Comparative study of gavage and intraperitoneal administration of gamma-oryzanol in alleviation/attenuation in a rat animal model of renal ischemia/reperfusion-induced injury. Iran J Basic Med Sci. 2021;24(2):175–83.
42. Penter L, Liu Y, Wolff JO, Yang L, Taing L, Jhaveri A, et al. Mechanisms of response and resistance to combined decitabine and ipilimumab for advanced myeloid disease. Blood. 2023;141(15):1817–30.
43. Satija R, Farrell JA, Gennert D, Schier AF, Regev A. Spatial reconstruction of single-cell gene expression data. Nat Biotechnol. 2015;33(5):495–502.
44. Korsunsky I, Millard N, Fan J, Slowikowski K, Zhang F, Wei K, et al. Fast, sensitive and accurate integration of single-cell data with Harmony. Nat Methods. 2019;16(12):1289–96.
45. Trapnell C, Cacchiarelli D, Grimsby J, Pokharel P, Li S, Morse M, et al. The dynamics and regulators of cell fate decisions are revealed by pseudotemporal ordering of single cells. Nat Biotechnol. 2014;32(4):381–6.

46. Cao J, Spielmann M, Qiu X, Huang X, Ibrahim DM, Hill AJ, et al. The single-cell transcriptional landscape of mammalian organogenesis. Nature. 2019;566(7745):496–502.
47. Chen T, Guestrin C. Xgboost: A scalable tree boosting system. 2016. In: Proceedings of the 22nd ACM SIGKDD international conference on knowledge discovery and data mining – KDD, pp. 785–94.
48. Alvarez MJ. Virtual inference of protein-activity by enriched regulon analysis. Bioconductor version: Release (311). 2016;10:B9.
49. Smoot ME, Ono K, Ruscheinski J, Wang PL, Ideker T. Cytoscape 28: new features for data integration and network visualization. Bioinformatics. 2011;27(3):431–2.
50. Yu G, Wang LG, Han Y, He QY. clusterProfiler: an R package for comparing biological themes among gene clusters. OMICS. 2012;16(5):284–7.
51. Hänzelmann S, Castelo R, Guinney J. GSVA: gene set variation analysis for microarray and RNA-seq data. BMC Bioinform. 2013;14:7.
52. Love MI, Huber W, Anders S. Moderated estimation of fold change and dispersion for RNA-seq data with DESeq2. Genome Biol. 2014;15(12):550.
53. Kumar L, Futschik ME. Mfuzz: a software package for soft clustering of microarray data. Bioinformation. 2007;2(1):5–7.
54. García-Prat L, Kaufmann KB, Schneiter F, Voisin V, Murison A, Chen J, et al. TFEB-mediated endolysosomal activity controls human hematopoietic stem cell fate. Cell Stem Cell. 2021;28(10):1838-50.e10.
55. Tang Z, Li C, Kang B, Gao G, Li C, Zhang Z. GEPIA: a web server for cancer and normal gene expression profiling and interactive analyses. Nucleic Acids Res. 2017;45(W1):W98–102.
56. Popova S. Human haematopoietic stem cell heterogeneity in postnatal haematopoiesis and ontogeny. UCL (University College London) (2021).
57. Watt SM, Bühring HJ, Simmons PJ, Zannettino AWC. The stem cell revolution: on the role of CD164 as a human stem cell marker. NPJ Regen Med. 2021;6(1):33.
58. Calvanese V, Mikkola HKA. The genesis of human hematopoietic stem cells. Blood. 2023;142(6):519–32.
59. Ng SW, Mitchell A, Kennedy JA, Chen WC, McLeod J, Ibrahimova N, et al. A 17-gene stemness score for rapid determination of risk in acute leukaemia. Nature. 2016;540(7633):433–7.
60. Khan O, Giles JR, McDonald S, Manne S, Ngiow SF, Patel KP, et al. TOX transcriptionally and epigenetically programs CD8+ T cell exhaustion. Nature. 2019;571(7764):211–8.
61. Sharma S, Gurudutta GU, Satija NK, Pati S, Afrin F, Gupta P, et al. Stem cell c-KIT and HOXB4 genes: critical roles and mechanisms in self-renewal, proliferation, and differentiation. Stem Cells Dev. 2006;15(6):755–78.
62. Bastl K. Unravelling the role of CDK6 and STAT5 in NPM-ALK-driven malignant transformation (2021)
63. Uckelmann HJ, Haarer EL, Takeda R, Wong EM, Hatton C, Marinaccio C, et al. Mutant NPM1 directly regulates oncogenic transcription in acute myeloid leukemia. Cancer Discov. 2023;13(3):746–65.
64. Ge T, Gu X, Jia R, Ge S, Chai P, Zhuang A, et al. Crosstalk between metabolic reprogramming and epigenetics in cancer: updates on mechanisms and therapeutic opportunities. Cancer Commun (Lond). 2022;42(11):1049–82.
65. Xia P, Ji X, Yan L, Lian S, Chen Z, Luo Y. Roles of S100A8, S100A9 and S100A12 in infection, inflammation and immunity. Immunology. 2024;171(3):365–76.
66. Zhang X, Zhang W, Ma SF, Miasniakova G, Sergueeva A, Ammosova T, et al. Iron deficiency modifies gene expression variation induced by augmented hypoxia sensing. Blood Cells Mol Dis. 2014;52(1):35–45.
67. Dong Q, Xiu Y, Wang Y, Hodgson C, Borcherding N, Jordan C, et al. HSF1 is a driver of leukemia stem cell self-renewal in acute myeloid leukemia. Nat Commun. 2022;13(1):6107.
68. Fei MY, Wang Y, Chang BH, Xue K, Dong F, Huang D, et al. The non-cell-autonomous function of ID1 promotes AML progression via ANGPTL7 from the microenvironment. Blood. 2023;142(10):903–17.
69. Yang G, Yang X. Smad4-mediated TGF-β signaling in tumorigenesis. Int J Biol Sci. 2010;6(1):1.
70. Wang JX, Zeng Q, Chen L, Du JC, Yan XL, Yuan HF, et al. SPINDLIN1 promotes cancer cell proliferation through activation of WNT/TCF-4 signaling. Mol Cancer Res. 2012;10(3):326–35.
71. Li L, Yang Q, Jiang Y, Yang W, Jiang Y, Li X, et al. Interplay and cooperation between SREBF1 and master transcription factors regulate lipid metabolism and tumor-promoting pathways in squamous cancer. Nat Commun. 2021;12(1):4362.
72. Russo RC, Garcia CC, Teixeira MM, Amaral FA. The CXCL8/IL-8 chemokine family and its receptors in inflammatory diseases. Expert Rev Clin Immunol. 2014;10(5):593–619.
73. Deng T, Shen P, Li A, Zhang Z, Yang H, Deng X, et al. CCDC65 as a new potential tumor suppressor induced by metformin inhibits activation of AKT1 via ubiquitination of ENO1 in gastric cancer. Theranostics. 2021;11(16):8112–28.
74. Hong J, Guo F, Lu SY, Shen C, Ma D, Zhang X, et al. F. nucleatum targets lncRNA ENO1-IT1 to promote glycolysis and oncogenesis in colorectal cancer. Gut. 2021;70(11):2123–37.
75. Huang CK, Lv L, Chen H, Sun Y, Ping Y. ENO1 promotes immunosuppression and tumor growth in pancreatic cancer. Clin Transl Oncol. 2023;25(7):2250–64.
76. Sun L, Suo C, Zhang T, Shen S, Gu X, Qiu S, et al. ENO1 promotes liver carcinogenesis through YAP1-dependent arachidonic acid metabolism. Nat Chem Biol. 2023;19(12):1492–503.
77. Shu X, Cao KY, Liu HQ, Yu L, Sun LX, Yang ZH, et al. Alpha-enolase (ENO1), identified as an antigen to monoclonal antibody 12C7, promotes the self-renewal and malignant phenotype of lung cancer stem cells by AMPK/mTOR pathway. Stem Cell Res Ther. 2021;12(1):119.
78. Zhang L, Wang H, Dong X. Diagnostic value of α-enolase expression and serum α-enolase autoantibody levels in lung cancer. J Bras Pneumol. 2018;44(1):18–23.
79. Shih NY, Lai HL, Chang GC, Lin HC, Wu YC, Liu JM, et al. Anti-α-enolase autoantibodies are down-regulated in advanced cancer patients. Jpn J Clin Oncol. 2010;40(7):663–9.
80. Liu Y, Li H, Liu Y, Zhu Z. MiR-22-3p targeting alpha-enolase 1 regulates the proliferation of retinoblastoma cells. Biomed Pharmacother. 2018;105:805–12.
81. Tsai ST, Chien IH, Shen WH, Kuo YZ, Jin YT, Wong TY, et al. ENO1, a potential prognostic head and neck cancer marker, promotes transformation partly via chemokine CCL20 induction. Eur J Cancer. 2010;46(9):1712–23.
82. Ray A, Song Y, Du T, Chauhan D, Anderson KC. Preclinical validation of Alpha-Enolase (ENO1) as a novel immunometabolic target in multiple myeloma. Oncogene. 2020;39(13):2786–96.
83. Yao Y, Li F, Huang J, Jin J, Wang H. Leukemia stem cell-bone marrow microenvironment interplay in acute myeloid leukemia development. Exp Hematol Oncol. 2021;10(1):39.
84. Niu J, Peng D, Liu L. Drug resistance mechanisms of acute myeloid leukemia stem cells. Front Oncol. 2022;12:896426.
85. Raff T, Brüggemann M. Leukemia-initiating cells in acute lymphoblastic leukemia. Cancer Stem Cells. 2014. https://doi.org/10.1002/9781118356203.ch12.
86. Chen K, Zhang C, Ling S, Wei R, Wang J, Xu X. The metabolic flexibility of quiescent CSC: implications for chemotherapy resistance. Cell Death Dis. 2021;12(9):835.

Publisher's Note